Jurnal Kejuruteraan 38(2) 2026: 635-648
https://doi.org/10.17576/jkukm-2026-38(2)-14

# Wear and Hardness of Thixoformed A356/Graphene Nanoplatelets Composites Fabricated via Stir Casting

Nur Farah Bazilah Wakhi Anuar[a,b*], Mohd Zaidi Omar[b], Mohd Shukor Salleh[a], Wan Fathul Hakim W. Zamri[b] & Afifah Md Ali[b]

[a]*Fakulti Teknologi dan Kejuruteraan Industri dan Pembuatan, Universiti Teknikal Malaysia Melaka, Hang Tuah Jaya, Durian Tunggal, 76100 Melaka, Malaysia,*

[b]*Faculty of Engineering and Built Environment, Universiti Kebangsaan Malaysia, 43600 Selangor, Malaysia*

[*]*Corresponding author: nurfarah@utem.edu.my*

*Received 4 July 2025, Received in revised form 29 November 2025*
*Accepted 29 December 2025, Available online 30 March 2026*

ABSTRACT

*The imperative to diminish emissions has propelled the automotive sector towards the use of lightweight materials, thereby augmenting interest in aluminium metal matrix composites for applications where strength and wear resistance are essential. Aluminium–silicon alloys, such as A356, remain important light alloys in the automotive field due to their low density and castability. Hence, the influence of the combined stir-casting and thixoforming process on the microstructure, hardness, and wear properties of graphene-reinforced A356 aluminium metal matrix composites was investigated. The microstructure results indicate that the stirring process transforms dendritic α-Al to a non-dendritic and rosette-like structure. The thixoforming process generates the coarse equiaxed α-Al and refined eutectic silicon. This morphological transformation, combined with the addition of GNPs, improves the mechanical strength and wear resistance of the composites. The findings demonstrated significant improvements in material performance, including a hardness test that reveals a 36% improvement in the thixoformed A356/GNP composite compared with the unreinforced alloy. The wear rate of the thixoformed A356/GNPs composite decreased by 23.4% and 19% under 10 N and 50 N normal loads, respectively, compared to that of the A356 alloy. The enhancement in hardness and wear resistance of the composites was attributed to both the efficient dispersion of GNPs with appropriate content in the composites and the presence of graphene as a self-lubricant on the composite's sliding surface. This study contributes to the development of stir casting and thixoforming as semi-solid processing methods for composite materials with enhanced wear resistance for engineering applications.*

*Keywords: Aluminium composites; graphene; thixoforming; wear; microstructure*

## INTRODUCTION

Numerous industries widely utilise aluminium alloys as lightweight materials, given their advantageous features, such as high specific strength and reduced density (Abdo et al. 2021; Eisay & Turan 2025), high potential for recycling (Klobčar et al. 2022), good corrosion resistance (Toor & Zafar 2022), and beneficial thermal conductivity (Linn et al. 2023). Nevertheless, the demand for advanced parts with weight reduction, cost reduction, and exhibiting high wear resistance in automotive applications necessitates the use of advanced materials (Singh et al. 2023). For this reason, aluminium metal matrix composites (AMMCs) have been developed as newly reinforced composite materials using nanoparticles. The properties of AMMCs are enhanced with superior mechanical strength, outstanding resistance to corrosive and abrasive degradation, and enhanced stability at elevated temperatures, making them in high demand in terms of quality in the automotive industry compared to metal matrices (Dhruv & N Parmar 2025; Samal et al. 2020; S. K. Sharma et al. 2024; Singh et al. 2023). Conventional reinforcement materials, including $Al_2O_3$ (He et al. 2022), $B_4C$ (Kabil et al. 2022), SiC (Ji et al. 2023), TiC (Bedolla-Becerril et al. 2022), graphite (Liu et al. 2023) and $ZrO_2$ (Mudzaffar et al. 2025)

are employed to enhance the performance of metal matrix composites beyond that of the unreinforced matrix. Nevertheless, conventional reinforcement materials often employ micro-sized materials. Hence, introducing carbonaceous materials as nanoscale reinforcements, such as graphene and carbon nanotubes, is promising for advanced high-performance applications.

Graphene comprises a single-atom-thick crystal layer where carbon atoms in graphene self-organise into a honeycomb lattice characterised by maximal 2D packing efficiency (Hasan et al. 2022). The combination of graphene's low density, high surface area, superior physical properties, and exceptional thermal performance makes it a highly effective reinforcement for aluminium metal matrix. Sharma et al. (2023) reported that the compressive strength and hardness properties of graphene nanoplatelets (GNPs)/Al nanocomposites have significantly improved compared to samples of pure aluminium with a proper number of GNPs. Numerous studies show that the GNPs powder tends to agglomerate as the GNPs content increases after 0.5 wt.% (Baig et al. 2020; Khanna et al. 2023). Furthermore, the remarkable mechanical strength of graphene contributes to its excellent resistance to wear behaviour and has been widely reported in various studies (Pekok et al. 2023; Şenyurt et al. 2024). Recent studies have shown the benefits of introducing graphene as a solid lubricant in aluminium metal matrix composites to improve mechanical characteristics and wear behaviour, as documented in a few related publications (Hsieh et al. 2020; Manjunath Naik et al. 2021; Sachit et al. 2023). Srivyas & Charoo (2022) synthesised $Al_2O_3$/GNPs/Al-Si composites and tested them under unlubricated sliding contact at a normal load of 10 N. They reported that GNPs reinforcement significantly modified tribological responses, but wear resistance decreased proportionally with elevated GNP content. Işik et al. (2024) conducted wear tests on graphene-reinforced Al7075 at 5 N and 10 N normal loads to quantify wear rates. The results showed that incorporating graphene reduces the wear rate of the composite by 21.9% compared to the Al7075 base alloy under a low load of 5 N. Therefore, graphene warrants significantly more research attention than other reinforcements for solid lubrication applications

Currently, solid-state powder metallurgy is a prevalent manufacturing approach for developing graphene-reinforced aluminium matrix composites (Borand & Uzunsoy 2022). Attaining a consistent distribution of graphene elements within matrix particles presents challenges frequently when using mechanical milling (Hanizam et al. 2020; Sharma et al. 2023). Additionally, prolonged ball milling periods can destroy the primary crystalline structure of the graphene particles (Yu et al. 2019). Other than that, the casting process is a typical liquid-state process for preparing aluminium metal matrix composites (Deng et al. 2020; Kotteda et al. 2024; Pazhani et al. 2023). Nevertheless, the abundant difference in density between aluminium and graphene leads to agglomerations and porosities in the composite. The stir-cast processing method offers numerous superior performance characteristics relative to alternative processing techniques for producing large-scale materials, including cost-effectiveness, ease of use, adaptability, versatility across various materials, and an efficient production rate. Nonetheless, there are significant disadvantages to the stir casting technique, including the gas entrapment due to the application of mechanical vortex and local solidification (Shivalingaiah et al. 2022). Consequently, secondary processing is implemented, elevating the mechanical and wear resistance of cast composite materials.

The semi-solid metal process is currently employed to produce metal products (Flemings, 1991). The semi-solid metal process has also garnered increasing interest as a potentially advantageous technology for enhancing the mechanical characteristics and structures of aluminium metal matrix composites (Li et al., 2022). Bobić et al. (2014) employed compo-casting as a semi-solid process to synthesise hybrid SiC- and graphite-reinforced A356 aluminium composites. This compo-casting process restructures α-Al from dendritic to non-dendritic configurations, yielding a hardness superior to that of conventional A356 aluminium alloy. Furthermore, the thixoforming process actively exploits thixotropic behaviour to generate non-dendritic microstructures, establishing it as a key semi-solid processing route (Kapranos 2019; Md Ali et al. 2024). The thixoforming process offers numerous advantages, including diminished porosity, lower energy consumption, and an extended lifespan of moulds (Chang et al. 2021). Samat et al. (2021) developed a modified Al-Si-Cu alloy with varying alloying element percentages and fabricated it using the thixoforming process. The processed alloy exhibits enhanced mechanical properties, with increases of 4 % in hardness, 49 % in yield strength, and 68 % in ultimate tensile strength compared to the gravity-cast alloy. Wang & Chen (2024) report that the formation of a fine equiaxed microstructure in graphene oxide-reinforced metal matrix composites after the thixoforming process improves hardness and tensile properties by 21.8% and 18.8%, respectively, compared to the unreinforced matrix. Alhawari et al. (2024) demonstrated that the thixoforming process alters the microstructure, yielding spheroidal α-Al grains embedded in a homogeneously dispersed Si phase. Consequently, this transformation significantly improves the tribological properties, specifically reducing volume loss and the coefficient of friction while enhancing wear resistance in

A319 alloy. Therefore, thixoforming emerges as a viable manufacturing route for aluminium matrix composites.

Tribological characterisation of thixoformed A356/GNPs composites under variable normal loads is notably limited. Hence, thixoforming is adopted to produce A356/GNPs composite specimens. Subsequent analysis quantifies the influence of thixoforming on the microstructural features and hardness properties of the alloy and composites. Progressing to tribological evaluation, the investigation focuses on the wear response in both as-cast and thixoformed conditions. This integrated analysis delivers valuable contributions to the literature on semi-solid manufacturing of advanced GNPs-reinforced metal composites.

## METHODOLOGY

### PROCEDURE OF FABRICATED MATERIAL

A356 aluminium alloy, analysed as the base material, exhibited the following composition: 7.38% Si, 0.26% Mg, 0.05% Cu, 0.013% Ni, 0.007% Zn, 0.19% Mn, 0.25% Fe, and 91.85% Al by weight percentage (wt.%). This experiment utilised graphene nanoplatelets (GNPs) as a reinforcement material with a consistent weight percentage of 0.3 wt.%. The consistent 0.3 wt.% GNPs were designated based on the previously conducted experiment (Md Ali et al. 2022; Wakhi Anuar et al. 2024). Pure magnesium (Mg) with a 1 wt.% content was applied to reduce the surface tension between GNPs and A356 alloy in the melt. Aluminium foil encapsulated the GNP and Mg powder mixture, which was subsequently preheated at 200 °C prior to its incorporation into the molten alloy.

The experimental procedure involved heating and melting 400 g of A356 alloy in a crucible, achieving a peak temperature of 700 °C and maintaining this temperature for 5 minutes to ensure complete melting. Then, the temperature was decreased and remained at 650 before the wrap was injected into the melt using the plunger and the melt was mechanically agitated at 500 rpm for 5 min. The composite melt was mechanically stirred, poured into a preheated steel die, and cast into a cylindrical billet with 25 mm diameter and 100 mm height as thixoforming feedstock**.** A thixoforming machine with T30 80 kHz 35 kW was employed for the thixoforming process. The semi-solid temperature with a 50% liquid fraction, as the requirement temperature for the thixoforming process, was selected from differential scanning calorimetry (DSC) data, as illustrated in Figure 1. The billet was reheated in the induction coil until its temperature reached 581 . The experimental setup incorporated real-time temperature monitoring of the reheating billet using a K-type thermocouple. Subsequently, a 20 kN hydraulic press rammed the reheated billet into the steel mould. The thixoformed sample was ejected from the steel mould and air-quenched to room temperature. The overall process route for producing the composites is schematically shown in Figure 2. In addition, Table 1 provides an overview of the processes employed in this study, along with their corresponding nomenclature.

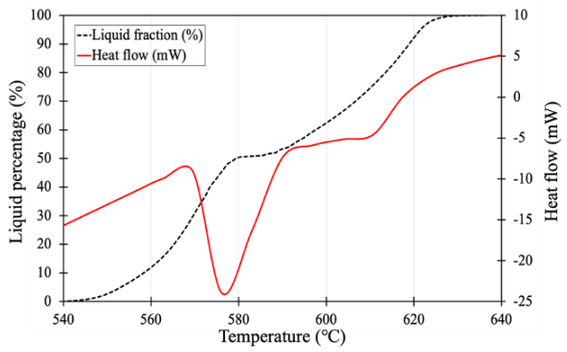


FIGURE 1. Phase characteristics of DSC heating curves and corresponding liquid fraction behaviour of composites

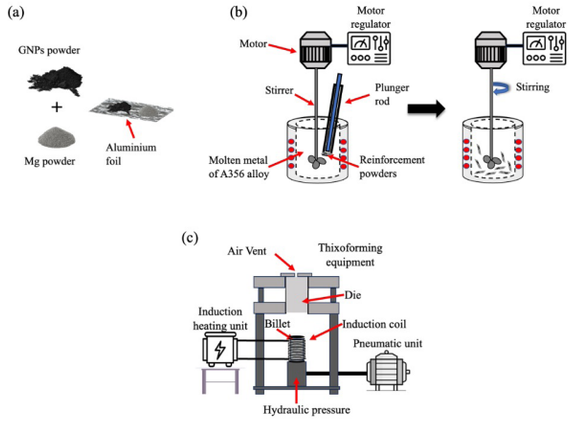


FIGURE 2. Schematic representation of fabricated composites (a) preparation of GNPs powder and Mg powder in aluminium foil, (b) stir casting process and (c) thixoforming process

TABLE 1. Processes and corresponding nomenclature in this study

| No. | Material | Process | Nomenclature |
|---|---|---|---|
| 1. | A356 | As-received | A356 alloy |
| 2. | A356 + GNPs | Stir-casting | As-cast A356/GNPs |
| 3. | A356 | Stir-casting + thixoforming | Thixoformed A356 |
| 4. | A356 + GNPs | Stir-casting + thixoforming | Thixoformed A356/GNPs |

## CHARACTERIZATION METHOD

The samples were prepared as 10 mm diameter sections with 20 mm length for microstructural observation, hardness testing and density measurement. The sectioned surface of samples was grinding with silicon carbide paper to P2400, polished to 1 μm with a diamond solution, and etched with Keller's reagent. Next, Nikon optical microscopy (OM) and field-emission scanning electron microscopy (FESEM) with an accelerating voltage of 10 kV were utilised to investigate the etched surface of the sample and obtain microstructural analysis. The HMV-G Vickers hardness tester was employed for measurements under a 9.807 N load and 10 s dwell time, in accordance with ASTM E384-17. At least ten indentations were conducted for each sample for reliability. The density of the samples was assessed with a Densimeter MD-300, and the experimental density was determined through the application of Archimedes' principle. Density measurements were conducted on each fabricated sample at the top, centre, and bottom, with 3 readings taken at each location, and the results were subsequently averaged.

This study performed dry sliding wear characterisation via a pin-on-disc tribometer, adhering strictly to ASTM G99 standards. Subsequently, this investigation designated normal load, sliding speed, and sliding distance as key control variables for wear characterisation. EN32 steel with a surface roughness (Ra) 0.3 μm served as the counterface material throughout the wear test. The input parameters operated in the wear test are introduced in Table 2. Prior to testing, all 10 mm × 20 mm pin samples were polished to attain a surface finish of 0.2 μm Ra. A calibrated microbalance (Mettler Toledo XSR, ±0.0001 g) was used to determine mass differentials before and after sliding tests, enabling the calculation of volumetric wear loss and specific wear rate (SWR). The load cell continuously monitored friction during the sliding test and transmitted the data to the computer system. Three measurements of each parameter were conducted to obtain reliable results. Field-emission scanning electron microscopy (FESEM) was used to characterise worn-surface morphologies and determine the dominant wear mechanisms at an accelerating voltage of 15 kV.

TABLE 2. Input parameters used in the wear test using the pin-on-disc type

| Input Parameter | Value |
|---|---|
| Normal load (N) | 10, 50 |
| Sliding speed (m/s) | 1.0 |
| Sliding distance (m) | 3000 |
| Temperature | Ambient |
| Counterface disc | EN32 steel (62 HRC) |

## RESULTS AND DISCUSSION

### OBSERVATION OF MICROSTRUCTURE

Notably, Figure 3 depicts the microstructural transformation of the A356 alloy alongside the as-cast A356/GNPs composite, the thixoformed A356 alloy, and the thixoformed A356/GNPs composite, using FESEM. The transformation of microstructures was essential for understanding the enhancement of the hardness and wear properties of the fabricated A356/GNPs composite. Figure 3(a) and Figure 3(b) clearly illustrate the long-dendritic structure of the α-Al phase in the A356 alloy, with characteristic encapsulation by the eutectic Si phase. Following mechanical stirring, Figure 3(c) and Figure 3(d) reveal the resultant microstructural modification in the as-cast A356/GNPs composite. Critically, the as-cast A356/GNPs composite exhibits a non-dendritic morphology alongside an irregular rosette-like structure in the α-Al phase, arising directly from mechanical stirring. The application of external mechanical forces from the stirring process breaks up the dendritic arms and forms an island structure.

Furthermore, the presence of GNPs modifies the development of the α-Al phase, leading to its characteristic non-uniform globular morphology. Additionally, the α-Al phase develops its irregular morphology through dynamic interactions between turbulent melt behaviour and particulate inertia during processing. Thus, the combination of turbulence disrupts the development of globular structures. However, the irregular globular morphology proved favourable for subsequent thixoforming.

Figure 3(e) and Figure 3(f) reveal the transformation of the $\alpha$-Al phase after the thixoforming process of the A356 alloy. The $\alpha$-Al phase becomes coarser and globular due to the reheating process, while the eutectic Si becomes finer with a combination of globular and fibrous-like structures. Arif et al. (2020) identify that the globular structure of the $\alpha$-Al phase of the alloy changes as a result of the imposition of compressive force throughout the thixoforming procedure. Intriguingly, the development of the globular α-Al phase synergises with eutectic Si refinement to enhance mechanical performance in metal alloys (Aziz et al. 2024; Putra et al. 2022).

Furthermore, the microstructure resulting from the thixoforming process applied to the A356/GNPs composite was presented in Figure 3(g) and Figure 3(h). The figure reveals that the rosette-like structure of the $\alpha$-Al phase in the thixoformed composite becomes non-uniform, equiaxed, and coarser than the $\alpha$-Al phase in Figure 3(e) and Figure 3(f). The applied thixoforming pressure and dissolution of the eutectic Si that occur during isothermal holding jointly drive the merging of the $\alpha$-Al phase,

elucidating the observed behaviour (Hanizam et al. 2020). Moreover, the occurrence of GNPs in the boundary region hindered the establishment of a consistent spherical or globular structure of the $\alpha$-Al phase.

Furthermore, the microstructure reveals the distribution and rearrangement of fine fibrous-like eutectic Si particles surrounding the $\alpha$-Al phase. However, prior research has shown that GNP improves the eutectics in the associated aluminium matrix composite. Andilab et al. (2022) established that GNP particles concentrated preferentially surrounding the eutectic Si phase. Consequently, the presence of the GNPs particles could also enhance the refinement of eutectic Si. Hence, the presence of the coarse and non-uniform equiaxed $\alpha$-Al phase, including fine fibrous eutectic Si, was anticipated to increase the mechanical properties and wear performance of the composite.

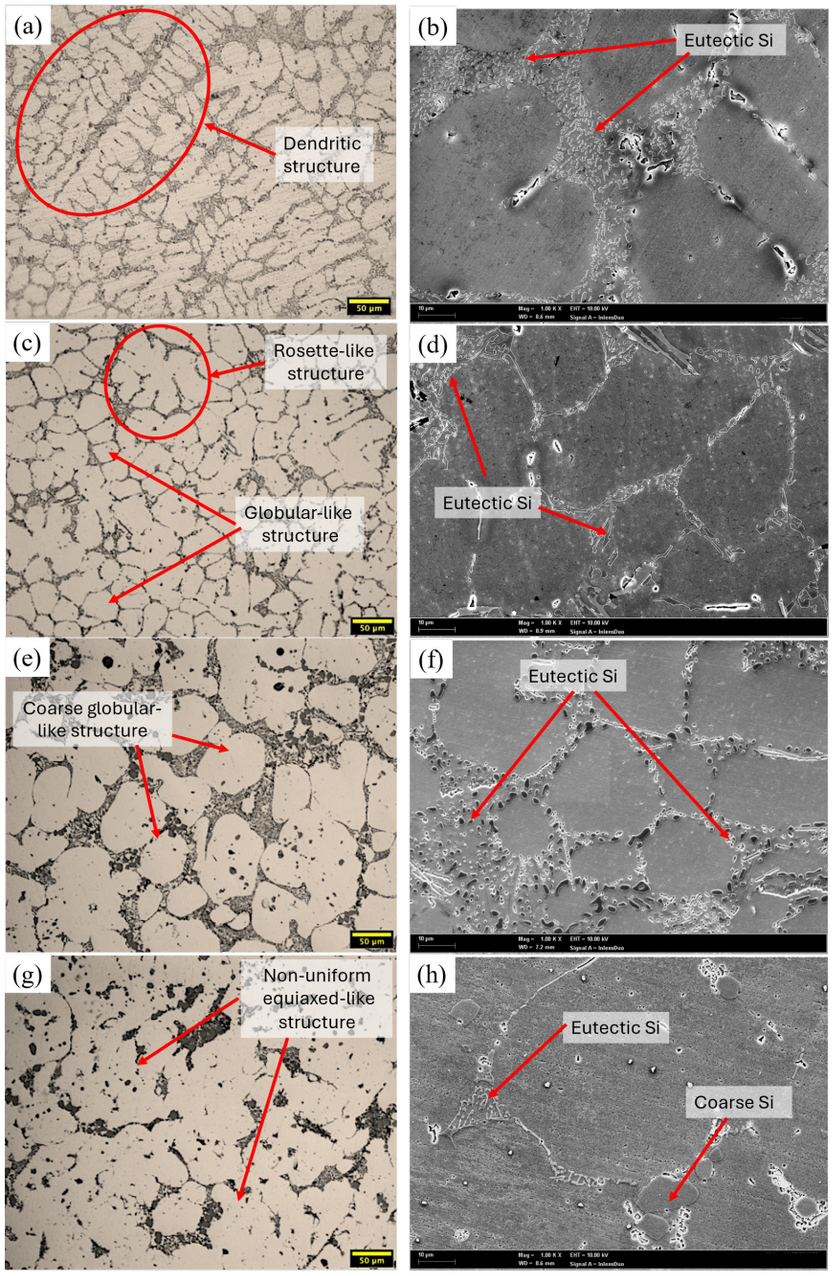


FIGURE 3. Optical micrographs and FESEM image for (a)(b) A356 alloy, (c)(d) as-cast A356/GNPs composite after mechanical stirring, (e)(f) thixoformed A356 alloy and (g)(h) thixoformed A356/GNPs composite. (a)(c)(e)(g) were captured using an optical microscope at 200× magnification. (b)(d)(f)(h) were obtained using FESEM at 1000× magnification (10 kV)

Figure 4 illustrates the XRD patterns for as-cast A356 alloy, thixoformed A356 alloy, as-cast A356/GNPs composite and thixoformed A356/GNPs composite. The detection of Al peaks corresponding to the (111), (200), (220), (311), and (222) planes establishes that α-Al is a significant constituent of the composite microstructure. The XRD results also identified (200), (220), and (311) peaks of Si for all samples. Interestingly, the intensity of the Al peak reduced by almost half after adding graphene, indicating a change in crystallinity due to lattice-cell distortion (Sachit et al. 2023). However, the absence of detectable graphene peaks in both as-cast and thixoformed composites indicates that the GNPs concentration is beyond the XRD detection limit (Şenel & Gürbüz 2020). Numerous studies have identified the detection of carbon by XRD (Kolev et al. 2023; Srivyas & Charoo 2022; Wang et al. 2024; Zhang et al. 2022), with a high graphene content of more than 1 wt. % GNPs. Nevertheless, the small carbide peaks were detected and indexed to $Al_4C_3$. Additionally, the secondary phases were unrevealed in the XRD pattern due to the general scans conducted in this investigation.

Zhang et al. (2022) reported the formation of limited $Al_4C_3$ carbides, predominantly segregated along grain boundaries, subsequent to composite fabrication. It is widely recognised that the development of $Al_4C_3$ carbide is facilitated by graphene defects or the chemical reactions between carbon and aluminium. In addition, elevated temperatures facilitate an interfacial reaction between graphene and aluminium, leading to the formation of a brittle carbide phase. High-temperature conditions and defects in carbon planes primarily influence the extent of the $Al_4C_3$-forming interfacial reaction (Hsieh et al. 2020). Numerous researchers have discovered that the formation of the carbide phase leads to impairment of the mechanical properties and wear behaviour (Keshavarz et al., 2025; Kotteda et al., 2024). However, the presence of nano-$Al_4C_3$ particles at grain boundaries promotes pinning, thereby improving the mechanical characteristics of these aluminium composites (Lazarova et al., 2022; Wei et al., 2023). Moreover, the diminutive presence of $Al_4C_3$ enhances the wettability between aluminium and carbon (Di Egidio et al. 2023). Therefore, the development of nanoscale carbides without excess promotes load transfer and reduces interfacial slip at the graphene-aluminium interface, thereby increasing the composite's strength.

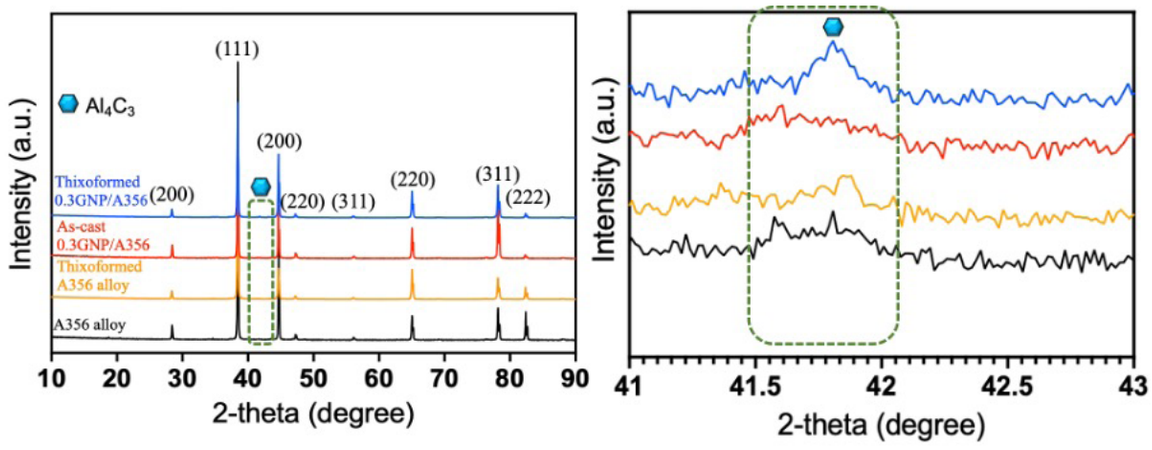


FIGURE 4. XRD pattern of as-cast A356 alloy, thixoformed A356 alloy, as-cast A356/GNPs composite and thixoformed A356/GNPs composite

## DENSITY AND HARDNESS PROPERTIES

Figure 5 presents experimental density and hardness measurements for all samples, where the composite's density critically influences material performance. As observed, the experimental density of as-cast A356/GNPs slightly reduces by 0.04 % compared to that of as-cast A356 alloys. The density advantage of graphene (2.26 g/cm³) over aluminium (2.7 g/cm³) is a key factor in lowering the overall composite density (Naik et al. 2022). Accordingly, reduced composite density is directly attributable to the inherent reactivity profile of incorporated reinforcements.

However, the experimental density of thixoformed A356 alloy and thixoformed GNP/A356 composite was higher than that of the as-cast samples. The results indicate that the experimental density of the thixoformed alloy and thixoformed composites was increased by 0.41 % and 0.34 %, respectively, compared to the A356 alloy. Zhang et al. (2024) discovered that the application of thixoforming resulted in a reduction in porosity and an increase in the density of the fabricated composites. Arendarchuck et al. (2023) further demonstrated that thixoforming increased

the density of A380/NbC matrix composites by 0.74% relative to their as-cast composites. Porosity notably reduces the mechanical integrity and wear performance of composites by introducing local stress concentrations and hindering load transfer between the graphene phase and the A356 matrix (Sharma et al. 2024). Thus, thixoforming was an adequate process for enhancing a composite's mechanical strength by reducing or preventing porosity defects and improving chemical uniformity.

The as-cast A356/GNPs composite (85.6 ± 2.11 HV) exhibited 35.8% higher hardness than the as-cast A356 alloy (63.0 ± 3.3 HV) and 13.6% greater hardness than the thixoformed A356 alloy (75.3 ± 2.7 HV). It demonstrates that incorporating GNPs into the alloys imparts a significant enhancement of hardness in the composite material. Wang et al. 2024) identify the hardness increment from 47.8 HV to 61.6 HV after adding 2 wt.% GNSs to aluminium alloy. Kotteda et al. (2024) also determined the increment of maximum hardness to 95.6 HV after adding 2 wt.% GNPs to the AA2024 alloy. Subsequently, Further processing via thixoforming elevated the A356/GNPs composite hardness to 95.4 ± 1.8 HV. The thixoforming generates a hardness increment through three mechanisms: optimising the GNPs reinforcement distribution, reducing porosity, and significantly refining the grain structure. Moreover, graphene possesses an intrinsically lower thermal expansion coefficient (CTE) than aluminium. The immense CTE mismatches between GNPs (~ $1 \times 10^{-6}$ $K^{-1}$) and A356 alloy (~ $2.1 \times 10^{-5}$ $K^{-1}$) (Md Ali et al. 2022), resulting in multidirectional thermal stress at the interface between GNPs and A356 alloys during the thixoforming reheating process. Additionally, the large specific area of graphene acts as a pinning platform, and precipitate formation was the reason for hardness improvement. The improvement in density also led to increased hardness and wear behaviour. Hence, adding GNPs with a low content of 0.3 wt.% and applying the thixoforming process substantially enhances composite hardness.

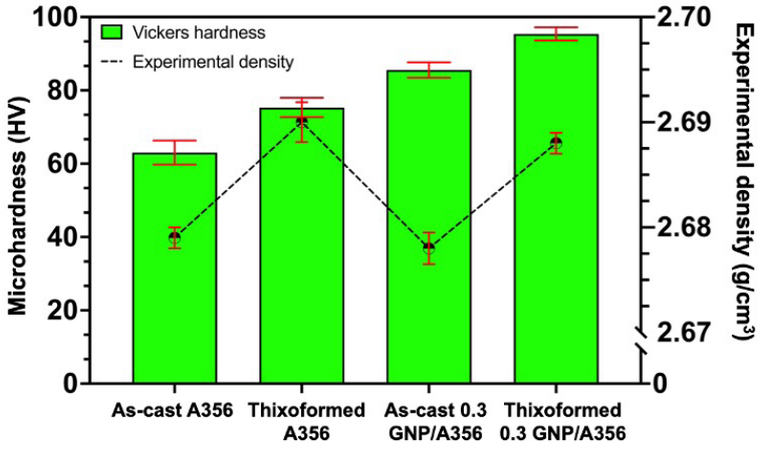


FIGURE 5. The hardness and experimental density of the sample for each process

## WEAR ANALYSIS

Figure 6 illustrates the volume loss, specific wear rate (SWR), and average coefficient of friction (COF) of the sample for each process under 10 N and 50 N loading conditions. Figure 6(a) demonstrates that the corresponding volume loss increases under elevated loading in both as-cast and thixoformed composite materials. This phenomenon aligns with Archard's law, which exemplifies Archard's wear principle, where the volume loss scales linearly with increasing applied force (Abdelgnei et al. 2020). The contact surface area increases as the load increases, whereas the gripping process between surface deformation and asperities increases. Accordingly, the results demonstrate that increasing the load elevates volume loss across all composite samples. Nevertheless, volume loss measurements revealed that the thixoformed A356/GNPs composites experienced less material loss than the alloy or the as-cast A356/GNPs composites.

Figure 6(b) illustrates the relationship of SWR to the normal load applied for the samples. At a load of 10 N, the SWR for the thixoformed A356/GNPs composite was determined to be $11.16 \times 10^{-5}$ $mm^3/(N.m)$. Comparatively, the SWR for the as-cast A356/GNPs composite was $12.69 \times 10^{-5}$ $mm^3/N.m$. The results indicate a reduction in SWR by 23.35% and 12.84% for the thixoformed and as-cast composites, respectively, compared to the SWR of the as-cast A356 alloy ($14.56 \times 10^{-5}$ $mm^3/(N.m)$). The results show

that applying a 50 N load yields a specific wear rate of 6.47 × $10^{-5}$ $mm^3$/(N.m) for the thixoformed A356/GNPs composite, whereas the as-cast composite exhibits a higher rate of 7.05 × $10^{-5}$ $mm^3$/(N.m). These values represent reductions of 19.02 % and 11.76 %, respectively, compared to the as-cast A356 alloy (7.99 × $10^{-5}$ $mm^3$/(N.m)) under a 50 N normal load. The analysis demonstrates that SWR declines progressively as load rises throughout the samples. Chak & Chattopadhyay (2021) identified that the wear rate of GNPs-reinforced Al7075 composites significantly reduces as the normal load increases. The applied load during sliding induces strain hardening, ultimately decreasing the material's wear rate (Atta et al. 2022). Additionally, hardness measurements have a significant impact on the SWR outcomes across composite materials. As composite hardness reliably determines SWR performance, Figure 5 confirms enhanced hardness in thixoformed A356/GNPs composites. This improvement originates from the microstructural transformation and the integration of GNPs, resulting in the lowest wear rates.

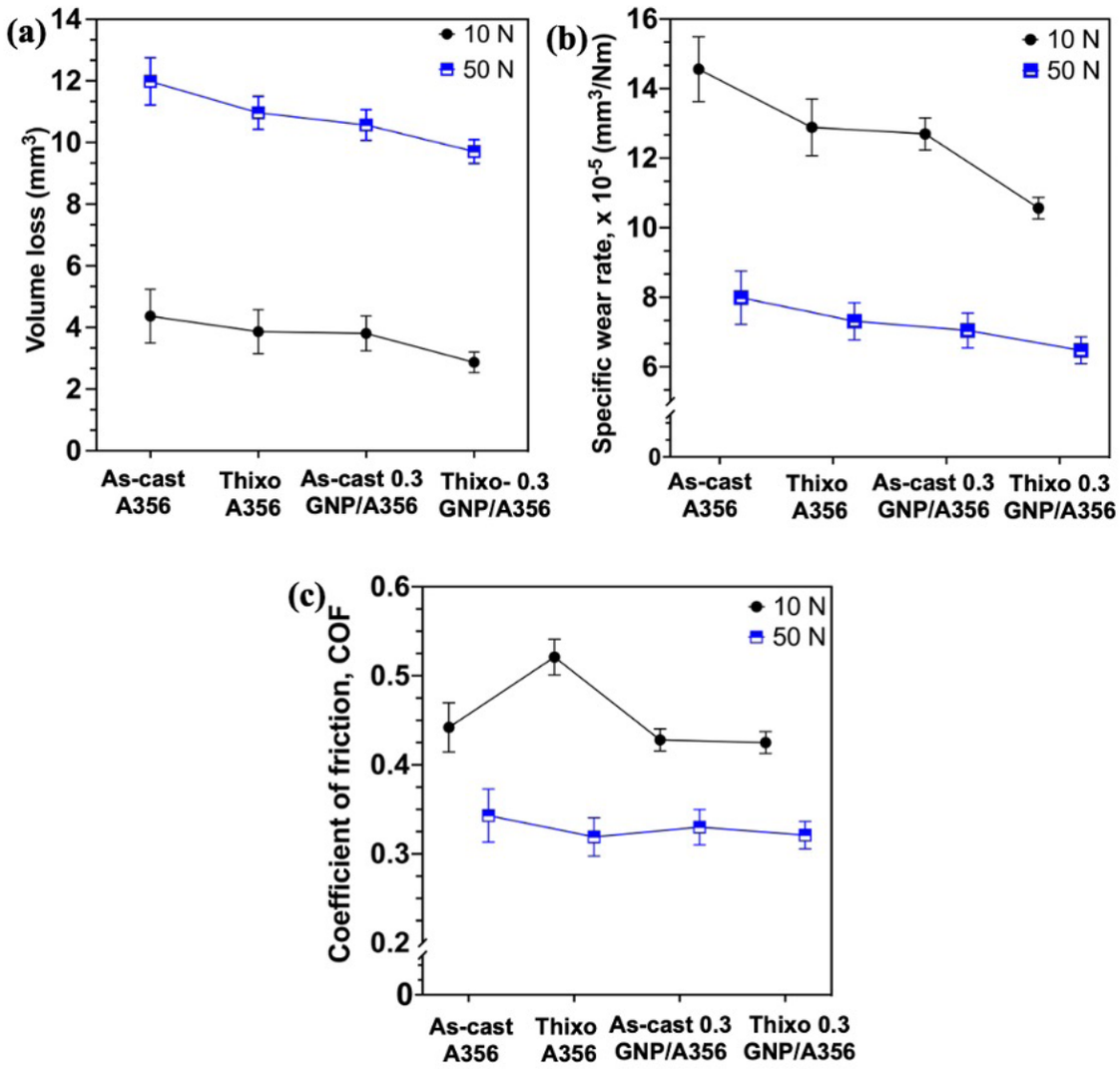


FIGURE 6. (A) Volume loss, (b) SWR, and (c) COF for all samples at each process under normal loads of 10 N and 50 N

Generally, harder materials commonly exhibit greater wear resistance than those with lower hardness values. Archard's principle elucidates the inverse correlation between the rate of wear and the hardness of a specific material (Demirtas et al. 2022; Valizade & Farhat 2024). Additionally, the slight presence of an $Al_4C_3$ as the carbide phase enhances the material's hardness by inhibiting the dislocation movement (Turan et al. 2021). Progressive loading increases volume loss uniformly, resulting from the extensive removal of the soft Al matrix phase. In contrast, specific wear rates decrease consistently under elevated loads. The presence of GNPs as reinforcement, which function as load-bearing particles and self-lubricating elements, further mitigates the unmediated contact of the composite matrix against the sliding surface (Zheng et al., 2020).

With increasing applied normal load, the pressure applied to the surface of the sample becomes higher, causing the load-bearing element to function at its maximum to prevent the volume of the sample from being continuously removed. Increasing the normal load elevates the sample surface temperature, and the difficulty in removing the sample increases due to plastic deformation. The formation of plastic deformation under a high normal load induces an enhancement in the hardness of the subsurface of the sample (Alhawari et al. 2024). In addition, the high hardness of the subsurface sample prevents significant removal of its surface. However, the absence of reinforcement material in the A356 alloy prevented the sample surface from withstanding the high pressure applied during the sliding process—a crack formed on the unprotected surface, resulting in large-volume removal of the A356 alloy. The α-Al phase undergoes a microstructural transformation during thixoforming of the A356 alloy, resulting in a uniform distribution of Si around the matrix phase (Yamamoto et al. 2020), thereby increasing resistance to normal loads. Therefore, volume wear loss and SWR were significantly affected differently during the sliding process. Thus, the combined influence of the fabrication process, the presence of GNPs as a self-lubricant, and the high hardness of the thixoformed A356/GNPS composite ultimately affects volume loss and SWR.

Figure 6(c) depicts the average COF of the samples for each process. It can be observed that COF was high at a load of 10 N for all samples. The actual surface contact area was inferior to the apparent surface area of the samples at a load of 10 N. Consequently, significant pressure was exerted on the small regions of contact asperities, which explains the high friction coefficient at a load of 10 N. The load of 50 N results in increased frictional heat at the interface of the contact surface, which softens the soft alloy. Subsequently, the shear strength decreased, and the COF dropped to a low value. Moreover, GNPs in composite samples can be recognised as third-body abrasives on the worn surface and possess load-bearing activity owing to the high hardness of thixoformed composites. Yu et al. (2021) identified that the surface roughness of composite-reinforced GNPs is higher due to the presence of GNPs and the increase in the mechanical interlocking of surfaces. It can be explained that the measured coefficient of friction was slightly higher for as-cast A356/GNPs composites than for the thixoformed alloy under a 50 N normal load in this study. Therefore, the wear tests demonstrate that the GNPs incorporation in the alloy was effective as a self-lubricant in the A356 composite. The comparison shows that applying the thixoforming process results in significantly higher wear resistance than conventional stir casting in A356/GNPs composite samples.

## WORN MORPHOLOGY

Figure 7 presents FESEM micrographs of worn surfaces for each processing condition after 10 N and 50 N wear testing. The worn surface of all samples exhibits a significant amount of particle debris when subjected to a load of 10 N. However, the worn surface of the thixoformed A356/GNPs composite was less damaged than that of other samples at normal loads of 10 N and 50 N, respectively. Figure 7(a) reveals dominant delamination and adhesive wear mechanisms on as-cast A356 alloy surfaces under a 10 N load. Low hardness simultaneously increases specific wear rates and enables delamination processes. The improved hardness obtained by thixoformed A356 alloy prevents the formation of numerous craters during sliding, resulting in fewer grooves and adhesives, as shown in Figure 7(b). Incorporating graphene reinforcement in A356 alloy substantially changes the appearance of the worn surface in the absence of craters. Figure 7(c) observes the formation of adhesive and parallel grooves on the worn surface for the as-cast A356/GNPs composite. There were numerous parallel groove formations where the wear debris was distributed along the frictional direction on the worn surface of the thixoformed GNPs-reinforced A356 composite, as shown in Figure 7(d). Nevertheless, low contact pressure generates converging grooves along the sliding directions in all samples.

Additionally, the surface area between the counterface and the samples was not directly in contact at a low normal load. Zhang et al. (2022) identify a narrow groove with shallow depth at a low normal load of 5 N. Hence, the penetration from asperities was shallow and unstable. Nevertheless, the worn surface analysis of the A356 alloy reveals that the soft matrix was unable to endure the low applied load, resulting in penetration.

Figure 7(e) reveals deep grooving and significant severe crater formation accompanied by delamination on as-cast A356 alloy worn surfaces under a 50 N load. Delamination occurs when the applied stresses at the worn surface exceed the composite strain limits, resulting in cracks beneath the worn surface (Karakoç 2023). The dendritic microstructure of A356 alloy, combined with the absence of GNPs, initiates surface cracks during sliding. Consequently, high-load counterface asperities penetrate deeply, inducing continuous spallation of the A356 alloy worn surface throughout the sliding process. The improved hardness in the thixoformed A356 alloy was beneficial from the formation of a non-dendritic microstructure, which prevents severe craters during sliding friction with a load of 50 N, as shown in Figure 7(f).

The as-cast A356/GNPs composite shows a less deep groove, and the thixoformed A356/GNPs composite sample shows a smooth surface with shallow grooves, as shown in Figure 7(g) and Figure 7(h), respectively, but both composite samples have fewer craters than the A356 alloy. Under the influence of shear pressures during friction sliding, GNPs located at the grain boundaries in the contact surface experienced compression and were expelled from the A356 alloy. Subsequently, the expelled GNP undergoes graphitisation and forms lubricious tribolayers on the wear track. The tribolayer's formation explains the volume loss, and the SWR of the thixoformed A356/GNPs composites was lower than that of the other samples at a high normal load. Moreover, expelled GNPs particles can potentially fill microvalleys or asperities on the worn surface, creating a smoother interface during sliding (Lin et al., 2023). Additionally, the GNPs struggled to maintain protection on the worn surface of the composites for an extended period during the sliding process. Hence, alongside the protective qualities of GNPs, the elevated hardness and high density of the thixoformed A356/GNPs composites increase their ability to resist deep ploughing under high pressure during wear sliding.

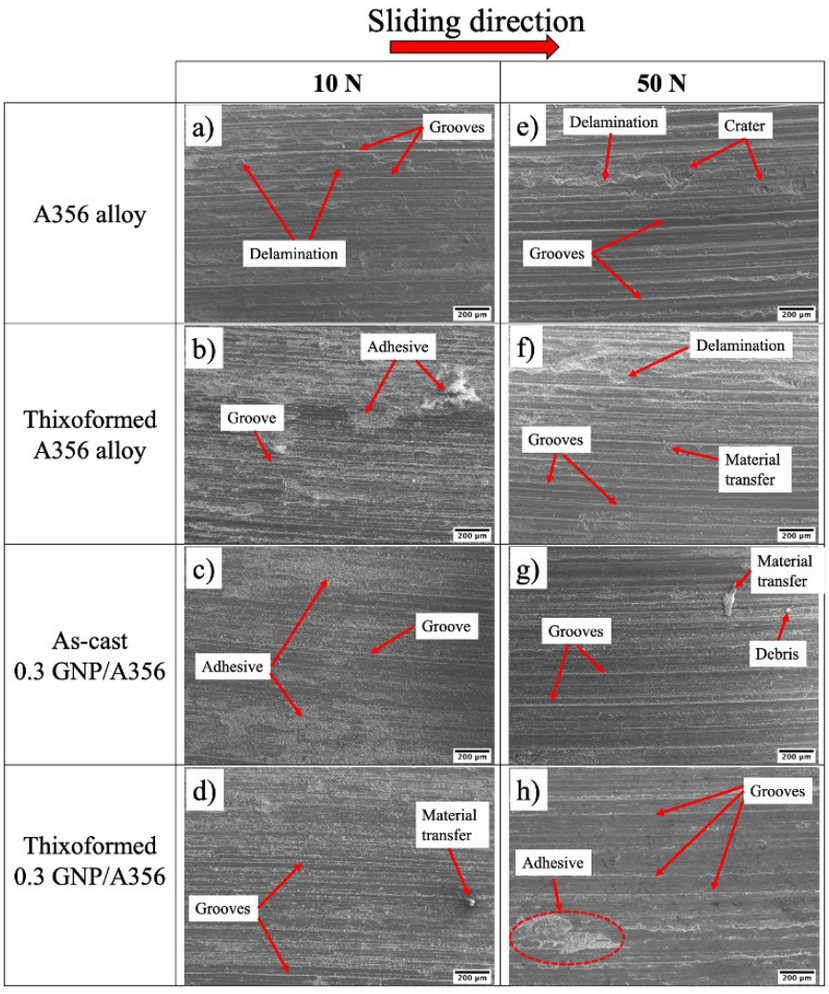


FIGURE 7. FESEM image of the worn surface for the alloy and composite at normal loads of 10 N and 50 N

Therefore, at both low (10 N) and high (50 N) loads, delamination and adhesive wear emerged as the dominant wear mechanisms in the as-cast A356 alloy, with minor abrasive wear. The wear mechanism for the thixoformed A356 alloy was adhesive and abrasive wear at a load of 10 N. Under 50 N loading, the thixoformed alloy transitions to abrasion-dominated wear mechanisms with minor adhesive mechanisms. Conversely, both the thixoformed alloy and A356/GNPs composites exhibit unified abrasive and adhesive wear mechanisms at 10 N. Significantly, abrasive wear mechanisms become the primary degradation mode for both thixoformed A356 alloy and thixoformed A356/GNPs composites at 50 N.

## CONCLUSION

This study details the fabrication of GNPs-reinforced A356 metal matrix composites using stir casting and thixoforming. Microstructure, hardness, and pin-on-disc sliding wear were conducted on GNPs-reinforced A356 composites. The influence of the normal load on wear characteristics was examined, and the overall conclusions are summarised as follows:

1. The thixoformed composites showed a transition from rosette-type to coarsened equiaxed α-Al grains, with finer eutectic silicon, contributing to improved mechanical and tribological responses.
2. Hardness increased by 35.8% in the as-cast composites and 51.4% in the thixoformed composites compared to A356 alloy, while there was a minimal $Al_4C_3$ formation in thixoformed composites detected by XRD.
3. The specific wear rate decreased continuously from a normal load of 10 N to 50 N. At a normal load of 10 N, the specific wear rate of the thixoformed composites was $11.16 \times 10^{-5}$ $mm^3/(N.m)$. The specific wear rate decreased continuously with increasing normal load of 50 N to $6.47 \times 10^{-5}$ $mm^3/(N.m)$.
4. The coefficient of friction of the material was in the range of 0.4–0.55 at a low normal load of 10 N. The coefficient of friction of the composites showed a reduction to the range of 0.3-0.4 at a high normal load of 50 N.
5. The wear mechanism of the thixoformed composites at a low load of 10 N was abrasive and adhesive wear. As the normal load increases to 50 N, the wear mechanisms of thixoformed composites transform to abrasive wear.

These outcomes confirm the enhancement in hardness and wear resistance imparted by GNP addition and combination process of stir casting and thixoforming, although the findings remain bounded by the stability of the tribolayers and the use of a single GNP content.

## ACKNOWLEDGEMENT

The authors would also like to thank Universiti Teknikal Malaysia Melaka (UTeM) for financial support under research grant PJP/2024/FTKIP/PERINTIS/SA0023 and Universiti Kebangsaan Malaysia (UKM) for the support of this study.

## DECLARATION OF COMPETING INTEREST

None.

## REFERENCES

Abdelgnei, M. A., Omar, M. Z., Ghazali, M. J., Mohammed, M. N. & Rashid, B. 2020. Dry sliding wear behaviour of thixoformed Al-5.7Si-2Cu-0.3 Mg alloys at high temperatures using Taguchi method. *Wear* 442-443: 203134.

Abdo, H. S., Seikh, A. H., Mohammed, J. A. & Soliman, M. S. 2021. Alloying elements effects on electrical conductivity and mechanical properties of newly fabricated Al based alloys produced by conventional casting process. *Materials* 14(14): 3971.

Alhawari, K. S., Omar, M. Z., Samat, S. & Aziz, A. M. 2024. Effect of magnesium addition consolidated by the thixoforming process on the wear properties of A319 alloy. *The International Journal of Advanced Manufacturing Technology* 131(7-8): 4327-4344.

Andilab, B., Emadi, P. & Ravindran, C. 2022. Casting and characterization of A319 aluminum alloy reinforced with graphene using hybrid semi-solid stirring and ultrasonic processing. *Materials* 15(20): 7232.

Arendarchuck, B. E., Fals, H. D. C. & Lourençato, L. A. 2023. Effect of thixoforming process and microstructural changes in the A380 matrix composite reinforced with NbC by the stir casting method. *JOM* 75(1): 184-194.

Arif, M. A. M., Omar, M. Z. & Saijuri, Z. 2020. Kebolehbentukan-tikso aloi 2014 dengan penambahan Si dan pengurangan Cu. *Sains Malaysiana* 49(1): 179-188.

Atta, M., Megahed, M. & Saber, D. 2022. Using ANN and OA techniques to determine the specific wear

rate effectors of A356 Al-Si/Al2O3 MMC. *Neural Computing and Applications* 34(17): 14373-14386.

Aziz, A. M., Omar, M. Z., Samat, S., Mohamed, I. F., Aripin, M. A. & Mazlan, M. R. 2024. Microstructural characterisation and high-cycle fatigue behaviour of semisolid Al-Si-Cu alloy. *International Journal of Metalcasting* 18(3): 2612-2623.

Baig, Z., Mamat, O., Mustapha, M. & Ali, S. 2020. Investigating sintering behavior of the graphene nanoplatelets (GNPs) reinforced aluminum nanocomposites via low energy solution ball milling. *Archives of Metallurgy and Materials* 65(2): 755-759.

Bedolla-Becerril, E., Garcia-Guerra, J., Lopez-Morelos, V. H., Garcia-Renteria, M. A., Falcon-Franco, L. A., Martinez-Landeros, V. H., García-Villarreal, S. & Flores-Villaseñor, S. E. 2022. Tribological behaviour of Al-2024/TiC metal matrix composites. *Coatings* 13(1): 77.

Bobić, I., Ružić, J., Bobić, B., Babić, M., Vencl, A. & Mitrović, S. 2014. Microstructural characterization and artificial aging of compo-casted hybrid A356/SiCp/Grp composites with graphite macroparticles. *Materials Science and Engineering: A* 612: 7-15.

Borand, G. & Uzunsoy, D. 2022. Fabrication of functionally graded few-layered graphene reinforced Al-4.5Cu alloy by powder metallurgy. *Journal of Alloys and Compounds* 923: 166348.

Chak, V. & Chattopadhyay, H. 2021. Synthesis of graphene-aluminium matrix nanocomposites: Mechanical and tribological properties. *Materials Science and Technology* 37(5): 467-477.

Chang, Z., Wang, X., Wu, Y., Peng, L. & Ding, W. 2021. Review on criteria for assessing the processability of semisolid alloys. *Materials Letters* 282: 128835.

Demirtas, M., Ivanov, K. V., Purcek, G. & Yanar, H. 2022. Enhancing mechanical and tribological properties of Ni3Al-15vol%TiC composite by high current pulsed electron beam irradiation. *Journal of Alloys and Compounds* 898: 162860.

Deng, Y., Pan, X., Zeng, G., Liu, J., Xiao, S. & Zhou, Z. 2020. Study on high-temperature wear and mechanism of Al-Si/graphite composites prepared by the die-casting process. *Industrial Lubrication and Tribology* 72(10): 1153-1158.

Dhruv, A. B. & Parmar, M. N. 2025. Effect of cryorolling on mechanical properties of Al alloy: A review. *Jurnal Kejuruteraan* 37(6): 2789-2808.

Di Egidio, G., Martini, C., Börjesson, J., Ghassemali, E., Ceschini, L. & Morri, A. 2023. Dry sliding behavior of AlSi10Mg alloy produced by laser-based powder bed fusion: Influence of heat treatment and microstructure. *Wear* 516-517: 204602.

Eisay, A. M. S. & Turan, M. E. 2025. Effect of reduced graphene oxide (rGO) on wear properties of Al7075 alloy produced via stir casting. *Diamond and Related Materials* 151: 111882.

Flemings, M. C. 1991. Behavior of metal alloys in the semisolid state. *Metallurgical Transactions A* 22(5): 957-981.

Hanizam, H., Salleh, M. S., Omar, M. Z., Sulong, A. B. & Arif, M. A. M. 2020. Effects of hybrid processing on microstructural and mechanical properties of thixoformed aluminum matrix composite. *Journal of Alloys and Compounds* 836: 155378.

Hasan, M. S., Wong, T., Rohatgi, P. K. & Nosonovsky, M. 2022. Analysis of the friction and wear of graphene reinforced aluminum metal matrix composites using machine learning models. *Tribology International* 170: 107527.

He, X., Lin, B., Zhang, W., Xiao, H. & Zhang, W. 2022. Microstructures and enhanced mechanical properties of (Al3Ti+Al2O3)/Al-Si composites with co-continuous network structure prepared by pressure infiltration. *Ceramics International* 48(24): 36824-36834.

Hsieh, C.-T., Ho, Y.-C., Wang, H., Sugiyama, S. & Yanagimoto, J. 2020. Mechanical and tribological characterization of nanostructured graphene sheets/A6061 composites fabricated by induction sintering and hot extrusion. *Materials Science and Engineering: A* 786: 138998.

Işik, E., Taşkin, A. & Şenel, M. C. 2025. Investigation of mechanical and tribological properties of Al7075-Al2O3-GNPs hybrid composites produced by powder metallurgy and induction hot pressing. *Journal of Materials Engineering and Performance* 34(9): 7309-7322.

Ji, X., Li, S., Zhang, X., Liu, L., Li, S., Gao, L., Li, X. & Wang, S. 2023. Influence of characteristic parameters of SiC reinforcements on mechanical properties of AlSi10Mg matrix composites by powder metallurgy. *Journal of Materials Research and Technology* 24: 6843-6853.

Kabil, A., Yüksel, Ç. & Çiğdem, M. 2022. Production and characterization of AA2014-B4C surface-modificated composite via the squeeze casting technique. *Revista de Metalurgia* 58(1): e217.

Kapranos, P. 2019. Thixoforming of aluminum A201: Expectations and fulfilment. *Solid State Phenomena* 285: 476-488.

Karakoç, H. 2023. Effect of SiC particle size on the mechanical and wear behavior of Al356 metal matrix composites. *Silicon* 15(15): 6729-6744.

Keshavarz, S., Asgharzadeh, H. & Farvizi, M. 2025. Microstructure, mechanical properties, and wear behavior of Al5083/GNPs nanocomposites prepared by powder metallurgy method. *Materials Science and Engineering: A* 929: 148120.

Khanna, V., Kumar, V., Bansal, S. A., Prakash, C., Ubaidullah, M., Shaikh, S. F., Pramanik, A., Basak, A. & Shankar, S. 2023. Fabrication of efficient aluminium/graphene nanosheets (Al-GNP) composite by powder metallurgy for strength

applications. *Journal of Materials Research and Technology* 22: 3402-3412.

Klobčar, D., Pušavec, F., Bračun, D., Garašić, I., Kožuh, Z., Vencl, A. & Trdan, U. 2022. Influence of friction riveting parameters on the dissimilar joint formation and strength. *Materials* 15(19): 6812.

Kolev, M., Lazarova, R., Petkov, V., Mourdjeva, Y. & Nihtianova, D. 2023. Investigating the effects of graphene nanoplatelets and Al4C3 on the tribological performance of aluminum-based nanocomposites. *Metals* 13(5): 943.

Kotteda, T. K., Kumar, M. & Kumar, P. 2024. Experimental insights and micrographical investigation on graphene nanoplatelet-reinforced aluminum cast composites. *The International Journal of Advanced Manufacturing Technology* 131(5-6): 2707-2718.

Kotteda, T. K., Kumar, M., Kumar, P. & Gupta, A. 2024. Development of forecast models on electrical discharge machined graphene nanoplatelets reinforced aluminum composite fabricated via stir casting route. *Cogent Engineering* 11(1).

Kotteda, T. K., Kumar, M., Kumar, P., Gupta, A. & Kalidindi, S. R. R. 2024. Mechanical and metallurgical behaviour of aluminum/graphene nanocomposites in fuselage applications. *Cogent Engineering* 11(1).

Lazarova, R., Mourdjeva, Y., Nihtianova, D., Stefanov, G. & Petkov, V. 2022. Fabrication and characterization of aluminum-graphene nano-platelets-nano-sized Al4C3 composite. *Metals* 12(12): 2057.

Li, N., Mao, W. & Geng, X. 2022. Preparation of semi-solid 6061 aluminum alloy slurry by serpentine channel pouring. *Transactions of Nonferrous Metals Society of China* 32(3): 739-749.

Lin, F., Ren, M., Wu, H., Lu, Y., Yang, M., Chen, Z. & Jiang, Z. 2023. Characterisation of microstructure, microhardness and tribological properties of Al matrix hybrid nanocomposites reinforced with B4C and in-situ GNSs. *Wear* 522: 204691.

Linn, Z. C., Min Swe, W. W., Soe, A. K. & Latt, A. K. 2023. Experimental and numerical analysis on the thermal performance of the aluminium absorber. *Tribology and Materials* 2(4): 162-171.

Liu, Y., Shi, Q., Qu, T., Zhou, M., Wen, F., Yue, N., Shi, F., Sun, C., Zhang, G. & Chen, G. 2023. Fabrication of graphite-reinforced 6201Al matrix composite with simultaneous enhancement of mechanical and electrical properties by multi-pass friction stir processing. *Journal of Alloys and Compounds* 967: 171835.

Manjunath Naik, H. R., Manjunath, L. H., Vishwanath, K., Avinash, L., Praveennath, G. K. & Sampath, K. P. 2021. Al/graphene/CNT hybrid composites: Hardness and sliding wear studies. *FME Transactions* 49(2): 414-421.

Manjunath, N. H. R., Manjunath, L. H., Vinayak, M., Manjunath, P. G. C., Kuldeep, K. S. & Lakshmikanthan, A. 2022. Effect of microstructure, mechanical and wear on Al-CNTs/graphene hybrid MMCs. *Advances in Materials and Processing Technologies* 8: 366-379.

Md Ali, A., Omar, M. Z., Salleh, M. S., Hashim, H., Mohamed, I. F. & Wakhi Anuar, N. F. B. 2022. Mechanical behaviour and morphology of thixoformed aluminium alloy reinforced by graphene. *Materials* 15(19).

Md Ali, A., Omar, M. Z., Salleh, M. S., Mohamed, I. F., Hashim, H. & Wakhi Anuar, N. F. B. 2024. Effect of heat treatment on the microstructures and mechanical properties of thixoformed graphene-reinforced aluminium alloy composite. *International Journal of Metalcasting* 18(2): 1695-1709.

Mudzaffar, R. N., Mohd Ali, A., Ibrahim Sktani, Z. D., Rejab, N. A., Mohd Zaki, H. H., Sarifuddin, N., Ahmad, Z., Ahmad Azhar, A. Z. & Abdullah, N. S. 2025. Mechanical performance of zirconia-toughened alumina composites: The dual role of nitinol as a toughening and sintering aid. *Jurnal Kejuruteraan* 37(7): 3471-3481.

Pazhani, A., Venkatraman, M., Anthony Xavior, M., Moganraj, A., Batako, A., Paulsamy, J., Jayaseelan, J., Anbalagan, A. & Shanthi Bavan, J. 2023. Synthesis and characterisation of graphene-reinforced AA 2014 MMC using squeeze casting method for lightweight aerospace structural applications. *Materials & Design* 230: 111990.

Pekok, M. A., Setchi, R., Ryan, M., Brousseau, E., Han, Q. & Gu, D. 2023. Graphene nanoplatelets reinforced Al-Cu-Mg composite fabricated using laser powder bed fusion: Microstructure, mechanical properties, and wear behaviour. *The International Journal of Advanced Manufacturing Technology* 128(3-4): 1597-1613.

Putra, A. G., Manaf, A. & Prajitno, D. H. 2022. The effect of Ca and thixoforming process on hardness and microstructure of Mg-Al-Zn alloys. *Journal of Materials Research and Technology* 19: 643-652.

Sachit, T. S., Bongale, A., Kumar, S. & Jadhav, P. 2023. Wear performance analysis of B4C and graphene particles reinforced Al-Cu alloy based composites using Taguchi method. *Journal of the Mechanical Behavior of Materials* 32(1).

Samal, P., Vundavilli, P. R., Meher, A. & Mahapatra, M. M. 2020. Recent progress in aluminum metal matrix composites: A review on processing, mechanical and wear properties. *Journal of Manufacturing Processes* 59: 131-152.

Samat, S., Omar, M. Z., Baghdadi, A. H., Mohamed, I. F. & Aziz, A. M. 2021. Mechanical properties and microstructures of a modified Al-Si-Cu alloy prepared by thixoforming process for automotive connecting rods. *Journal of Materials Research and Technology* 10: 1086-1102.

Şenel, M. C. & Gürbüz, M. 2020. Microstructure and wear behaviour of graphene-Si3N4 binary particle-reinforced aluminium hybrid composites. *Bulletin of Materials Science* 43(1): 148.

Şenyurt, B., Yaman, K. Ç. & Akçamlı, N. 2024. Few-layered graphene/Al-Cu alloy matrix composites: Mechanical, tribological and corrosion properties. *Materials Today Communications* 40: 110082.

Sharma, A., Morisada, Y. & Fujii, H. 2023. Interfacial microstructure and strengthening mechanisms of SPSed Al/GNP nanocomposite subjected to multi-pass friction stir processing. *Materials Characterization* 197: 112652.

Sharma, S. K., Gajević, S., Sharma, L. K., Pradhan, R., Sharma, Y., Miletić, I. & Stojanović, B. 2024. Progress in aluminum-based composites prepared by stir casting: Mechanical and tribological properties for automotive, aerospace, and military applications. *Lubricants* 12(12): 421.

Sharma, V., Mallick, A. & Kumar, K. 2023. Effect of graphene nanoplates on the mechanical and corrosion properties of aluminium nanocomposite fabricated by powder metallurgy. *Tribology and Materials* 2(4): 154-161.

Shivalingaiah, K., Nagarajaiah, V., Selvan, C., Kariappa, S., Chandrashekarappa, N., Lakshmikanthan, A., Chandrashekarappa, M. & Linul, E. 2022. Stir casting process analysis and optimization for better properties in Al-MWCNT-GR-based hybrid composites. *Metals* 12(8): 1297.

Singh, B., Kumar, I., Saxena, K. K., Mohammed, K. A., Ijaz Khan, M., Ben Moussa, S. & Shukhratovich Abdullaev, S. 2023. A future prospects and current scenario of aluminium metal matrix composites characteristics. *Alexandria Engineering Journal* 76: 1-17.

Srivyas, P. D. & Charoo, M. S. 2022. Tribological behavior of hybrid aluminum self-lubricating composites under dry sliding conditions at elevated temperature. *Tribology - Materials, Surfaces & Interfaces* 16(2): 153-167.

Toor, Z. S. & Zafar, M. M. 2022. Corrosion degradation of aluminium alloys using a computational framework. *Tribology and Materials* 1(4): 150-156.

Turan, M. E., Aydin, F., Sun, Y., Zengin, H. & Akinay, Y. 2021. Wear resistance and tribological properties of GNPs and MWCNT reinforced AlSi18CuNiMg alloys produced by stir casting. *Tribology International* 164: 107201.

Valizade, N. & Farhat, Z. 2024. A review on abrasive wear of aluminum composites: Mechanisms and influencing factors. *Journal of Composites Science* 8(4): 149.

Wakhi Anuar, N. F. B., Omar, M. Z., Salleh, M. S., Zamri, W. F. H. W. & Md Ali, A. 2024. Effect of graphene addition on microstructure and wear behaviour of the A356-based composite fabricated by thixoforming process. *Journal of Materials Research and Technology* 30: 4813-4831.

Wang, C., Zhu, X., Fan, Y., Liu, J., Xie, L., Jiang, C., Xiao, X., Wu, P. & You, X. 2024. Microstructure and properties of aluminum-graphene-SiC matrix composites after friction stir processing. *Materials* 17(5): 979.

Wang, L. & Chen, T. 2024. Optimizing microstructure and mechanical properties of bimodal-structured magnesium matrix composites by regulating the remelting time of powder thixoforming. *Journal of Alloys and Compounds* 987: 174211.

Wei, P., Chen, Z., Zhang, S., Li, B., Han, J. & Lu, B. 2023. Microstructure and mechanical properties of graphene and nano-zirconia reinforced AlSi10Mg composite fabricated by laser powder bed fusion. *Materials Science and Engineering: A* 864: 144574.

Yamamoto, K., Takahashi, M., Kamikubo, Y., Sugiura, Y., Iwasawa, S., Nakata, T. & Kamado, S. 2020. Effect of Mg content on age-hardening response, tensile properties, and microstructures of a T5-treated thixo-cast hypoeutectic Al-Si alloy. *Materials Science and Engineering: A* 798.

Yu, J., Zhao, Q., Huang, S., Zhao, Y., Zhou, Y., Lu, J., Dong, L. & Zhang, Y. 2021. Effect of sintering temperature on microstructure and properties of graphene nanoplatelets reinforced TC21 composites prepared by spark plasma sintering. *Journal of Alloys and Compounds* 879: 160346.

Yu, Z., Yang, W., Zhou, C., Zhang, N., Chao, Z., Liu, H., Cao, Y., Sun, Y., Shao, P. & Wu, G. 2019. Effect of ball milling time on graphene nanosheets reinforced Al6063 composite fabricated by pressure infiltration method. *Carbon* 141: 25-39.

Zhang, F., He, Z., Gao, W. & Zhan, Z. 2022. Mechanical behaviour of AA2024 composites reinforced by the synergistic strengthening effect of Al2Cu and GNPs. *Transactions of the Indian Institute of Metals* 75(11): 2959-2968.

Zhang, S., Chen, Z., Wei, P., Liu, W., Zou, Y., Lei, Y., Yao, S., Zhang, S., Lu, B. & Zhang, L. 2022. Wear properties of graphene/zirconia biphase nano-reinforced aluminium matrix composites prepared by SLM. *Materials Today Communications* 30: 103009.

Zhang, S., Wei, P., Chen, Z., Li, B., Huang, K., Zou, Y. & Lu, B. 2022. Graphene/ZrO2/aluminum alloy composite with enhanced strength and ductility fabricated by laser powder bed fusion. *Journal of Alloys and Compounds* 910: 164941.

Zhang, Z., Chen, T., Gao, M. & Zhang, J. 2024. Solution treatment of core-shell structured particle reinforced A356 composite prepared by powder thixoforming: Effects of partial remelting temperature. *Materials Chemistry and Physics* 315: 129065.

Zheng, K., Du, X., Qi, H., Zhao, T., Liu, F. & Sun, B. 2020. Sliding-wear behavior of aluminum-matrix composites reinforced with graphene and SiC nanoparticles. *Materiali in Tehnologije* 54(1): 41-48.